

1 Comment on "First records of syn-diagenetic non-tectonic
2 folding in Quaternary thermogene travertines caused by
3 hydrothermal incremental veining" by Billi et al.
4 *Tectonophysics* 700–701 (2017) 60–79

5
6 ** M. Cihat Alçiçek ¹, Hülya Alçiçek ¹, Erhan Altunel ², Concha Arenas ³, Paul
7 Bons ⁴, Andrea Brogi ^{5,*}, Enrico Capezzuoli ⁶, Tamara de Riese ⁴, Giovanna
8 Della Porta ⁷, Anna Gandin ⁸, Li Guo ⁹, Brian Jones ¹⁰, Volkan Karabacak ¹¹,
9 Stephen Kershaw ¹², Domenico Liotta ⁵, Andrea Mindszenty ¹³, Martyn Pedley
10 ¹⁴, Paola Ronchi ¹⁵, Rudy Swennen ¹⁶, Ugur Temiz ¹⁷

11
12 ¹ University of Pamukkale, Department of Geology, 20070, Denizli (Turkey)

13 ² University of Eskişehir Osmangazi, Department of Geological Engineering, 26040 Eskişehir (Turkey)

14
15 ³ University of Zaragoza, Department of Earth Sciences, Calle Pedro Cerbuna, 12. 50009 Zaragoza
16 (Spain).

17 ⁴ University of Tübingen, Department of Geosciences, Wilhelmstr. 56, 72074 Tübingen, (Germany)

18
19 ⁵ University of Bari, Department of Earth and Geoenvironmental Sciences. Via Orabona 4, 70125 Bari
20 (Italy)

21 ⁶ University of Perugia, Department of Physics and Geology. Via Pascoli, 06123 Perugia (Italy)

22 ⁷ University of Milan, Department of Earth Sciences. Via Mangiagalli 34, 20133, Milan (Italy)

23 ⁸ University of Siena, Department of Physics, Earth and Environmental Sciences, 53100 Siena, (Italy)

24 ⁹ CASP, 181A Huntingdon Road, Cambridge, CB3 0DH, (United Kingdom)

25 ¹⁰ University of Alberta, Department of Earth and Atmospheric Science, Edmonton , Alberta (Canada)

26 ¹¹ University of Eskişehir Osmangazi, Department of Geological Engineering, 26040 Eskişehir (Turkey)

27
28 ¹² University of Brunel, Department of Life Sciences, Uxbridge, Middlesex, UB8 3PH (United Kingdom)

29 ¹³ University of Eötvös L., Department of Physical and Applied Geology, 1117 Budapest, Pázmány P.
30 st.1/c (Hungary)

31 ¹⁴ University of Hull, Geology Group, School of Environmental Sciences, Hull, HU6 7RX (United Kingdom)

32 ¹⁵ ENI Upstream and Technical Services, Via Emilia 1, 20097, San Donato Milanese, (Italy)

33 ¹⁶ University of Leuven, Department of Earth and Environmental Sciences, KU Leuven, (Belgium)

34 ¹⁷ University of Bozok, Department of Geological Engineering, 66100 Yozgat (Turkey)

35

36 * Corresponding author: Tel. +39 080 5442576; e-mail: andrea.brogi@uniba.it

37 ** Authors are listed alphabetically

38 **Abstract**

39 Billi et al. (2017) proposed a new interpretation for the origin and internal
40 structure of thermogene travertine deposits. On the basis of evidence from two
41 quarries located in southern Tuscany (Italy), they interpreted some travertine
42 beds as calcite veins and argued that undulating travertine beds formed by
43 syn-diagenetic (i.e. non-tectonic) folding that was caused by laterally-confined
44 volume expansion caused by incremental veining. They assumed that such a
45 process causes changes to the rock properties, including porosity reduction,
46 rock strengthening, and age rejuvenation. The interpretations by Billi et al.
47 (2017) challenge and question the current understanding and interpretation of
48 thermogene travertine deposits. This understanding, based on numerous
49 studies since the 1980s, is that these deposits form from thermal water flowing
50 downslope, and precipitating calcium carbonate. Here, we explain how the
51 comparison with active depositional systems is essential for the understanding
52 the origin of structures in older, inactive travertine deposits, such as those
53 studied by Billi et al. (2017). We further argue that the three-dimensional
54 setting of travertine deposits should be taken into account in order to discuss
55 the possible development of secondary structures. Indeed travertine deposition
56 on slopes typically leads to the formation of terraced morphologies with pools
57 bordered by rounded rims and separated from each other by steep walls. The
58 resulting three-dimensional structures can be misinterpreted as asymmetric
59 folds in two-dimensional views (i.e., in saw-cut walls of quarry). In this paper
60 we debate the interpretations offered by Billi et al. (2017) and their criteria to
61 recognise syn-diagenetic, non-tectonic folds in travertine deposits, and explain
62 why many of their ideas are questionable.

63

64

65 **Key words**

66 travertine facies, travertine depositional geometry, deformational processes, calcite veins,
67 enterolithic structures, age rejuvenation

68

69

70 **1. Introduction**

71 The recent literature on travertine (i.e. thermogene terrestrial carbonate) has
72 made use of this deposit as a proxy for palaeo-environmental (Bertini et al.
73 2008; Ricci et al., 2015) and climate change reconstructions (Sturchio et al.,
74 1994; D'Argenio et al. 1995; Rihs et al., 2000; Soligo et al., 2002; Mesci et al.,
75 2008; Faccenna et al., 2008; Zentmyer et al., 2008; Sierralta et al., 2010;
76 Brogi et al., 2010), neotectonic and palaeoseismological analyses (Altunel and
77 Hancock, 1993a, 1993b; Çakır, 1999; Hancock et al., 1999; Brogi, 2004;
78 Altunel and Karabacak, 2005; Uysal et al., 2007; 2009; Mesci et al., 2008;
79 Brogi and Capezzuoli, 2009, 2014; Temiz et al., 2009; 2013; Brogi et al.,
80 2010, 2012, 2014a, 2014b, 2016; Altunel and Karabacak, 2005; Uysal et al.,
81 2007; 2009; Hancock et al., 1999; Temiz et al., 2009; 2013; Temiz and
82 Eikenberg, 2011; Cakir, 1999; Mesci et al., 2008), geothermal exploration
83 (Navarro et al., 2011; Pasvanoğlu and Chandrasekharam, 2011; Alçiçek et al.
84 2016; Brogi et al., 2016; Alçiçek et al., 2017), elemental biomediation
85 processes analyses (Folk, 1994; Bonny and Jones, 2003; Fouke et al., 2003;
86 Rogerson et al., 2014), and natural CO₂ degassing evaluation (Shipton et al.,
87 2005; Uysal et al., 2011; Frery et al., 2016). These applications coupled with
88 the fact that travertine is a rare carbonate deposit, makes it a precious archive
89 of information from many different scientific perspectives. The conventional
90 approach for the study of these deposits requires many different mandatory
91 steps, including: (i) reconstruction of the three-dimensional geometry of the
92 travertine deposit and its evolution through time; (ii) reconstruction of the
93 depositional architectural setting of the different depositional stages; and (iii)
94 sedimentary facies analysis that includes interpretation of sedimentary facies,
95 their lateral relationships, and the processes associated with each depositional
96 setting. The latter step is critical because it allows the reconstruction of the
97 environmental features that controlled the travertine formation and the related
98 sedimentary processes dictating its origin. Accurate facies interpretation
99 depends on careful observations that follow a well-established methodology,
100 which has been fully documented in a considerable number of previous studies
101 (e.g. Chafetz and Folk, 1984; Guo and Riding, 1992, 1994, 1998; Chafetz and
102 Guidry, 1999; Pentecost, 2005; Jones and Renaut, 2010; Gandin and

103 Capezzuoli, 2014).

104 Failure to follow the established protocols can lead to misinterpretations. This
105 is, in our opinion, the case presented in the paper by Billi et al. (2017) who
106 analysed Pleistocene (thermogene) travertine deposits exposed in saw-cut
107 walls of two quarries (see also: Ronchi and Cruciani, 2015), located in
108 southern Tuscany (Italy). They interpreted structures in those walls as syn-
109 diagenetic, non-tectonic veins and folds and provided nine criteria for
110 discriminating secondary structures (i.e. post-depositional syn-diagenetic
111 processes such as veining, folding, or rejuvenation actions) from primary
112 structures (i.e. related to the sedimentary evolution) in travertine deposits. We
113 question these criteria, which in our view do not sufficiently take in to account
114 the present knowledge on travertine formation. Herein, our comments aim to
115 fill this gap and to favour a solid consideration of the comparison between
116 active and fossil travertine depositional systems.

117

118 **1.1 Questions for comments**

119 Billi et al. (2017, their Figs. 3, 4) argued that the syn-diagenetic (i.e. non-
120 tectonic) folding of travertine was the result of laterally-confining volume
121 expansion that was caused by incremental hydrothermal veining. Their idea,
122 based on the study of Gratier et al. (2012), implied that undulating travertine
123 beds are unreliable indicators of the sedimentary environment (and its
124 evolution through space and time) in which the travertine accumulated.
125 Furthermore, a consequence of their hydrothermal-veining interpretation is
126 age rejuvenation of travertine deposits with implications for geochronological
127 results and modification of travertine strength and porosity, and effective
128 impacts on permeability evaluations. On the basis of these considerations, Billi
129 et al. (2017) proposed "*a list of significant criteria to discriminate secondary
130 from primary structures and to identify rejuvenation processes*" to explain the
131 occurrence of: (i) radiometrically-dated structures that are younger than
132 overlying ones; (ii) downward growth of crystals; (iii) veins
133 overprinting/cutting through overlying or underlying beds; (iv) relicts of

134 primary porous travertine beds between radiating vein crystals; (v)
135 increasingly deformed primary structures such as beds or pores towards veins
136 and folds; (vi) bed-normal foliations and second-order folds nested inside
137 larger folds; (vii) polyphase folding including overturned folds with refolded
138 limbs; (viii) stylolite surfaces parallel and stylolite teeth normal to vein planes;
139 (ix) post-depositional non-karstic voids between folded and flat veins and
140 beds, outlining the occurrence of post-depositional detachment mechanisms
141 between adjacent beds. We criticize the interpretation of these points. The
142 following text is therefore organized in separate sections, each of which
143 focuses on those aspects of the interpretations that are crucial for a well-
144 constrained facies analysis and reconstruction of the depositional
145 environments. In so doing, we underline and stress the lessons that have been
146 learnt from the analysis of active travertine depositional systems, which
147 collectively provide clear insights into the processes that define the
148 depositional geometry and development of travertine deposits.

149

150 **2. Calcite veins *versus* travertine beds/layers (crystalline crusts)**

151 This section discusses the points 2 to 5 of the list of criteria provided by Billi et
152 al. (2017) for the interpretation of travertine deposits.

153 Billi et al. (2017) described the geometric relation between the porous
154 travertine beds and the growth direction of the constituent calcite crystals (Billi
155 et al., 2017, their Figs. 4d, 4e and 11d) in the crystalline travertine beds (also
156 termed crystalline crusts by Guo and Riding, 1998 and references therein).
157 Based on this, Billi et al. (2017) argued that the porous travertine beds formed
158 as a primary deposit, whereas the crystalline crusts developed as calcite veins
159 that post-dated deposition of the travertine. This interpretation challenges the
160 fact that crystalline crusts are primary carbonate precipitates that develop at
161 the depositional surface as a result of CO₂ degassing from carbonate-rich
162 waters during their flow (**Fig. 1**). Thus, crystalline crusts are formed as a
163 variety of calcite/aragonite crystals (feather, fan, dendrites; see Jones and
164 Renaut, 1995; 2010 for a review; Jones et al., 2000, 2005). Furthermore, this
165 clarifies the definition of travertine as a primary bedded thermogene deposit

166 (Chafetz and Folk, 1984; Jones and Renaut, 1995, 2008; Jones et al., 1996,
167 2000, 2005; Guo and Riding, 1998; Jones and Renaut, 1995, 2008; Jones et
168 al., 1996, 2000, 2005; Rainy and Jones, 2009; Gandin and Capezzuoli 2014;
169 Della Porta, 2005; Croci et al., 2016; Della Porta et al., 2017) where the
170 intercalation of porous (**Fig. 2**) and crystalline deposits is a characteristics of
171 travertine spring deposits (Riding, 1991; Pedley, 1990; Flügel, 2004;
172 Pentecost, 2005; Pedley, 2009; Brogi et al., 2010; Capezzuoli et al., 2014;
173 Pola et al 2013; Gandin and Capezzuoli, 2014; Gradzinski et al., 2014).

174 Veins (see Bons et al., 2012 for a review) in travertine deposits (**Fig. 3**) are
175 formed of different types of crystals (Altunel and Karabacak, 2005; Uysal et
176 al., 2009, 2011; Rimondi et al., 2015; Brogi et al., 2014a; Brogi et al., 2016)
177 and fill cracks that cut across layers (**Fig. 3a-f**) or follow bedding surfaces
178 (**Fig. 3g-i**) (e.g. Altunel and Hancock, 1993a, 1993b; Altunel and Karabacak,
179 2005; Mesci et al., 2008; Uysal et al., 2009; 2011; Brogi et al., 2016; Brogi et
180 al., 2017; Selçuk et al., 2017).

181 The growth of bed-parallel veins (i.e. sub-horizontal veins that opened against
182 the force of gravity) has been attributed to: i) the crystallization force of calcite
183 triggered by CO₂ degassing at depths of 1–10 m (Gratier et al., 2012); ii)
184 repeated injections of high-pressure hydrothermal fluids (pressure exceeding
185 the weight of the overlying rocks volume, Brogi et al., 2016) during seismic
186 events (Uysal et al., 2007; Altunel and Karabacak, 2005; Uysal et al., 2007;
187 Brogi and Capezzuoli, 2014; Brogi et al., 2017) and/or (iii) by climate induced
188 pressure variations within the geothermal reservoir at depth (Uysal et al.,
189 2009). The textures of such veins (**Fig. 4**), however, are completely different
190 from the ones reported by Billi et al. (2017, their Fig. 4e). In their case, the
191 veins are formed of needle-like crystals, rows of palisade, fibrous or prismatic
192 crystals, generally arranged in tight palisades with straight extinction or
193 clusters of ray-shaped fans (as described in Folk et al., 1985; Atabey 2002;
194 see also Flügel, 2004, Jones and Renaut, 2010, Gandin and Capezzuoli, 2014,
195 for review on the petrographic characteristics of calcite veins and travertine).

196 They are typical of precipitates associated with pools and terraces (**Figs 1 and**
197 **2**). Such crystalline layers typically consist of dense crystalline dendrites or
198 crusts (some could also be shrubs as illustrated in Tivoli, nearby Rome, Italy,

199 as documented by Erthal et al., 2017) that can laterally, or vertically, grade
200 into the porous deposits where numerous voids from bubbles and other origins
201 are present (**Fig. 2**). This arrangement is readily evident in present-day active
202 travertine deposits all over the world and defines well-documented depositional
203 geometries such as dams, rims, and terraces (e.g. Pamukkale, Turkey;
204 Mammoth Hot Springs, USA; Huanglong, China; Badab-e surt, Iran, Saturnia,
205 Italy; Rapolano Terme, Italy; see also Pentecost, 1995, 2005; Ford and Pedley,
206 1996 for a review). Similar depositional structures are present in caves, where
207 the same process can be active (rimstone dams; Ford and Williams 2007).
208 These well-documented relationships between porous and crystalline beds
209 (**Figs 2 and 5** for active and fossil examples, respectively) also include what
210 Billi et al. (2017, their Fig. 5a and 5b) described as “chimney-like veins”. In
211 their photographs, it is apparent that the brownish porous layers pass laterally
212 into the dense crystalline layers (“veins” in Billi et al., 2017), with visible
213 interfingering relationships. This cannot, however, be attributed to a
214 subsequent deformational event. Moreover, their Fig. 4f shows that the
215 boundary of the crystalline beds with the porous micritic deposits is diffuse,
216 underlining the absence of mechanical/physical discontinuities that would be
217 expected if this were caused by subsequent pressure-induced deformation as
218 proposed by Billi et al. (2017).
219 Finally, Billi et al. (2017) based most of their arguments on evaluation of the
220 direction of calcite crystals growth. Conversely, the criteria used to establish
221 the growth-orientation of the travertine beds should be considered with care,
222 because the fan-like crystal arrangement (**Fig. 1d-g**) may result in different
223 apparent directions within the same bed (e.g. Billi et al. 2017, their Figs S25
224 and S34).
225 Billi et al. (2017) suggested that the development of calcite veins caused the
226 reduction of primary porosity (their Fig. 5c), as indicated by the flattened
227 pores, which they assumed were originally almost spherical (see their section
228 3.1.3). It is important to stress, however, that the classical, spherical “coated
229 bubbles” found in many travertine deposits (Guo and Riding, 1998; Gandin,
230 2013; Gandin and Capezzuoli, 2014 for a review) are formed by the
231 encrustation of bubbles with a thin coating of calcite caused by CO₂ degassing

232 (see Schreiber et al., 1981; Chafetz et al., 1991 and Pentecost, 2005 for a
233 complete description of this depositional process). When this is the case, the
234 bubbles are externally characterized by thin calcite rims. Consequently, this
235 type of porosity is commonly concentrated in small volumes (**Fig. 2**).
236 Otherwise, most pores in travertine (as all the pores discussed in Billi et al.,
237 2017) are formed from photosynthetic oxygen that is produced by microbial
238 activity and are common in microbial deposits (e.g. Folk et al., 1985; Riding,
239 1991; Rainey and Jones, 2009). Given that these are not coated by a calcite
240 rim, their shape is highly variable (e.g. Gandin and Capezzuoli, 2014 for a
241 comparison) and reflects the balance among gas pressure, gravity, and weight
242 of the microbial mat. Thus, the pore shape cannot be used to evaluate
243 deformation in travertine deposits, because their initial shape is highly variable
244 and unpredictable. It follows that the interpretation of the crystalline beds as
245 calcite veins that postdated the original travertine deposits is difficult to
246 accept.

247

248

249 **3. 2D-view of crystalline crusts versus folded travertine**

250 Hereafter we discuss the points 6 and 8 of the list of criteria that Billi et al.
251 (2017) proposed for the interpretation of travertine deposits.

252 Billi et al. (2017) argued that undulations in the travertine beds are syn-
253 diagenetic folds that developed during the progressive and incremental
254 formation of syntaxial, bedding-parallel, calcite veins. In active spring
255 depositional environments (**Fig. 1**) the undulation in travertine deposits
256 (undulated layers) is a natural consequence of subaerial deposition on variably
257 inclined surfaces (i.e. slopes and dammed zones), through pools and rims,
258 producing terraced surfaces (**Fig. 2**). This is well constrained by three-
259 dimensional observations in most active and fossil travertine (and tufa)
260 depositional systems (Italy: Chafetz and Folk, 1984; Guo and Riding, 1998;
261 D'Argenio et al., 1981, D'Argenio and Ferreri, 1987,1988; Hungary: Scheuer
262 and Schweitzer, 1981; Kele et al., 2008; Claes et al., 2017, Török et al., 2017;
263 Turkey: Altunel and Hancock, 1993a; 1993b; Khatib et al. 2014; Lebatard et
264 al., 2014; Claes et al., 2015; Tunisia: Henchiri et al., 2017; China: Liu et al.,

265 1995; Lu et al., 2000; Central Italy: Capezzuoli et al., 2014; Della Porta,
266 2015; Croci et al., 2016; Della Porta et al., 2017; Violante et al., 1994a,
267 1994b; Central Western Carpathians, Slovakia: Gradzinski et al., 2014; USA:
268 Fouke et al., 2000; different places: Pentecost 2005; Alonso-Zarza and Tanner
269 2010; Arenas-Abad et al. 2010; Jones and Renaut 2010).

270 Taking a different viewpoint, Billi et al. (2017), evaluating geometries based on
271 2D-cross sections, interpreted the undulatory and terraced travertine beds as
272 asymmetric folds, and argued that the typical aggradational and slightly
273 progradational geometry of the pool/rims are the result of second-order folds.
274 They did not consider the well-established fact that travertines are self-
275 regulating systems, that can modify their own depositional environment, which
276 may result in changes in the attitude of the strata with, or even without, any
277 syn- or post-depositional tectonic deformation.

278 Ronchi and Cruciani (2015), who studied the same quarries as Billi et al.
279 (2017), interpreted the terraced travertine as an effect of the travertine
280 deposition on pre-existing slopes. Billi et al. (2017) did not provide convincing
281 reasons for modifying the interpretations proposed by Ronchi and Cruciani
282 (2015) and the numerous of studies from other areas that show the same
283 features (Chafetz and Folk, 1984; Guo and Riding, 1998; D'Argenio et al.
284 1981; Scheuer and Schweitzer, 1981; Altunel and Hancock, 1993a; Khatib et
285 al. 2014; Lebatard et al., 2014; Claes et al., 2015; HENCHIRI et al., 2017; Liu et
286 al., 1995; Lu et al., 2000; Pentecost, 2005 for a review; Capezzuoli et al.,
287 2014, Della Porta, 2015; Croci et al., 2016; Della Porta et al., 2017).

288 Billi et al. (2017, their Figs 5f and 5g) also described folds with evident hinge
289 thickening that affect the calcite veins. They proposed for a composite
290 deformational process, with initial formation of mostly sub-horizontal calcite
291 veins that was followed by folding of the previously developed veins and
292 parallel porous travertine beds. They also argued that there was a sub-
293 horizontal tectonic foliation developed in association with the second-order
294 folds developed only in the vertical fold limb of the first order structures (see
295 their Fig. 5g and 6). In addition, their Fig. S10 is meant to show refolded
296 structures resulting from at least two folding events, with deformation of the
297 limb of a larger overturned fold.

298 The folds, refolded folds, and related tectonic foliation proposed by Billi et al.
299 (2017) have already been unequivocally described as primary depositional
300 features (cf. Chafetz and Folk, 1984; Hammer et al., 2010), but they did not
301 discuss or refute this interpretation. The undulatory beds that they interpreted
302 as first-order folds (and refolded folds) are explained as an effect of the plane
303 view orientation in a travertine cascade environment (**Fig. 6a-b**). Their
304 "second order folds" and associated "axial planar tectonic foliations" (cf. their
305 Figs 6b, 6d and 6f) can be explained as microterraces (**Fig. 6c-e**) that formed
306 on spring slopes (e.g. "rimstone pool" of Warwick, 1952, to "terracette" of
307 Bargar, 1978 and Guerts et al., 1992; "minidams" of Pentecost 2005 and Jones
308 and Renaut 2010; "microterraces" in Hammer et al., 2010).

309 The 2D-features displayed on the quarry walls by Billi et al. (2017, their Fig. 5
310 and 6) are recognizable in all present-day depositional systems (**Fig. 2**). This
311 circumstance reinforces the argument that these are really vertical cross-
312 sections through fossil pool rims (i.e. microterraces) and cascades that formed
313 by natural (i.e. primary) sedimentary processes (**Fig. 6**); they are not
314 (second-order) folds as suggested by Billi et al. (2017). In addition, it should
315 also be remembered that the shape, size, and distance between micro- and
316 macro-terraces depend on local depositional features (e.g. Riding, 1991;
317 Pentecost 2005: see Fig. 16; Goldenfeld et al., 2006; Hammer et al. 2005,
318 2007, 2010; Veysey and Goldenfeld, 2008), not only for travertine, but also for
319 all flowstone deposits (speleothems, tufa, siliceous sinter).

320 Billi et al. (2017) claimed a further explanation for their minor folds. They
321 suggested that the process that produced the small-scale folding is analogous
322 to the process that produces enterolithic and/or tepee structures, which are
323 commonly found in evaporitic deposits. Enterolithic structures (i.e. irregular,
324 highly-non-cylindrical tight to open folds) are typical of sabkha environments
325 and cannot develop in travertine deposits. Such structures are produced by
326 localized changes in volume after evaporite deposition (cf. Gandin and Wright,
327 2007). This syn- to meta-depositional deformation is induced by the chemical
328 transformation of the sulphates, such as the swelling of anhydrite during
329 hydration to gypsum. Gypsum and anhydrite nodules form through the
330 capillary system within the upper phreatic zones beneath the sabkha surface,

331 displacing and replacing sediment under pressurized saline fluids that are
332 flowing through pores due to evaporative capillarity (Tucker, 1988; Warren,
333 1999, 2006; Flügel, 2004; Gandin and Wright, 2007). These intrasediment
334 crystals grow in a matrix of fine sediment (i.e. lime mud, clays), where the
335 nodules grow and coalesce to form the enterolithic structures. Thermogene
336 travertine, however, with primary precipitation of calcite/aragonite, has a
337 completely different chemical and mineralogical composition, as well as an
338 internal organisation, and its deposition occurs in totally different
339 environments. Thus, there is no basis for assuming that travertine deposits
340 may develop in the same manner as evaporites and therefore, extreme care
341 should be taken when comparing the two.

342

343 **3.1 Mechanics of travertine folding**

344 This section discusses the points 7 and 9 of the list of criteria proposed by Billi
345 et al. (2017).

346 Travertine forms at the subaerial surface, where deposition and lithification
347 processes are almost contemporaneous (Pentecost, 1995). Travertine is
348 composed largely of calcite and/or aragonite, carbonate minerals that are
349 brittle under low temperature conditions ($< 250^{\circ}\text{C}$, Rutter, 1972).
350 Furthermore, the maximum thickness of travertine in slope environments does
351 not exceed a few tens of meters as found in several areas worldwide
352 (Pentecost 1995; Guo et al., 1996; Hancock et al., 1999; Brogi, 2004; Brogi et
353 al., 2010; Ronchi and Cruciani, 2015; Khatib et al. 2014; Lebatard et al.,
354 2014; Claes et al., 2017). This implies that travertine can only be affected by
355 deformation at, or near the surface. It follows that the boundary conditions (P,
356 T and/or significant content of interstitial fluids) required to obtain highly non-
357 cylindrical folds (Billi et al., 2017, their Fig. 5j) are not present. In this view,
358 the flattened, squeezed, dragged pores as Billi et al. (2017) described close to
359 the fold hinges, veins and folded veins (Figs. 3b, 5c, d, S6, S11, S12, S14,
360 S23, and S35), are not the result of the folding mechanism but are primary
361 sedimentary features, as discussed above.

362 Second-order folds attributed to folding imply bedding viscosity contrast
363 and/or thickness variations of a flexural slip folding mechanism. This is

364 normally produced in a multi-layered succession, which does not seem to apply
365 to travertine formed by carbonate precipitation on a terraced slope. In order to
366 explain fold hinge thickening and occurrence of second-order folds and
367 foliations, Billi et al. (2017, their Figs. 5f, g, and 6) considered the Biot-
368 Ramberg's buckling equation (their Eq. 1). Billi et al. (2017) used the buckling
369 equation for single-layer folding and an assumed Newtonian viscosity to obtain
370 a viscosity contrast of about 1.5 to 4. They did not report the amplitudes of the
371 folds (A) in relation to the fold wavelength (λ), which is shorter than the arc
372 length (L) that they used. Although it is difficult to ascertain how layer
373 thicknesses (t) were defined in the multi-layer setting, it seems that a ratio of
374 $A/l \geq 0.25$ is a conservative estimate for the structures. Their reported L/t ratios
375 range from about 4 to 5. This can be converted to t/l ratios, using $l \geq 2/3 \cdot L$, in
376 the range of 0.1 to 0.25.

377 A/λ versus t/λ trends depend on the amount of shortening and viscosity
378 contrast (Fig. 6 in Schmalholz and Podladchikov, 2001; Fig. 2 in Llorens et al.,
379 2013). For single-layer folding, the range of measured ratios would indicate
380 $\geq 50\%$ shortening and a viscosity ratio between 25 and 250. At the very low
381 viscosity contrast, as used by Billi et al. (2017), folds grow very slowly in
382 amplitude as layer thickening dominates. To achieve $A/\lambda \gg 0.25$, a very high
383 strain would be required, but this would result in much higher t/λ ratios
384 ($\gg 0.5$) than the ones observed.

385 If the buckle fold theory were applicable (which we doubt), the viscosity
386 contrast between the layers in the travertine would need to be much higher
387 than that proposed by Billi et al. (2017). More importantly, the amount of
388 strain needed to achieve the high A/λ ratios would be well over 50%
389 shortening, or in case of constrained volume increase, $>100\%$ of layer length
390 increase by volume change. In addition, Billi et al. (2017, their Fig. S11) also
391 described bedding-parallel stylolites that are typically associated with
392 dissolution that takes place as a result of overburden loads during deep burial
393 and pressure solution (e.g. Bathurst, 1995; Rolland et al., 2012; Heap et al.,
394 2014; Koehn et al., 2016). Their development is related to the occurrence of
395 local rock mass heterogeneity, occurrence of interlayered/intracrystalline
396 water, dissolution and deposition of dissolved material in extensional veins,

397 and a sufficient lithostatic pressure. As shown by Sellier (1979), the pressure-
398 dissolution of calcite begins at a depth of about 300 m. In other cases,
399 stylolites have been documented at lesser burial depth, at about 90 m, but
400 only if the limestones have a high clay content (Schlanger, 1964). Taking into
401 account that the travertine deposits described by Billi et al. (2017) were not
402 buried to the depth needed for stylolite formation, we doubt that the structures
403 described by Billi et al. (2017) are stylolites. The 2D-view of the outcrop is
404 again at the base of this misunderstanding: features similar to stylolites can be
405 produced if the saw-cut walls are about orthogonal (or at high angle) to the
406 crystalline crust on slopes that were originally terraced (**Fig. 6c-e**).

407

408 **4. Travertine age rejuvenation**

409 This part is dedicated to the discussion of the point 1 of the list of criteria
410 provided by Billi et al. (2017), concerning the interpretation of the age of
411 travertine deposits.

412 Radiometric age dating of travertine is possible by analysis of the U/Th content
413 in the calcite molecules (Taylor and McLennan, 1995 and references therein).
414 U/Th dating of carbonates, younger than 500ka (Walker, 2005), is a sensitive
415 analysis that relies on carefully collected samples (Ku and Liang, 1985). The
416 best dates come from compact, non-porous samples (cf. Carrara et al., 1998;
417 Brogi et al., 2010). Porous travertine samples can be problematical because
418 younger calcite and/or aragonite cements found in the pores may have formed
419 at any time after deposition. The presence of these cement phases can
420 seriously affect the isotopic and geochronological results. Billi et al. (2017, Fig.
421 7) showed inconsistent age-dating results through a travertine section
422 encompassing "veins" and "porous" travertine. The "inconsistent" ages
423 (samples CP15_8, CP14_2, ST1 and ST3) were used as criteria to validate the
424 "vein" formation. Two samples of travertine layers (lower photo in their Fig.
425 7b) show an inverted age order, whereas, other samples (upper photos in their
426 Fig. 7b) show upward younging. Following the principle they adopted,
427 however, only one "vein" sample (CP15_8, at the lowest position) is younger

428 than the sample that represents the supposed hosting travertine (CP14_25),
429 whereas the other “veins” produced older (CP15_1; CP14_5), or coeval
430 (considering the error range: CP14_2) ages. Interestingly, the uppermost
431 sample of their travertine (ST4) is younger than the underlying (CP13_1-5;
432 CP13_1-4) or quasi coeval (considering the error range: ST1; ST3) to the
433 underlying ST1 and ST3. Although problems seem to exist with the travertine
434 ages, Billi et al. (2017) did not discuss any possible source of errors. The age
435 results, irrespective of how reliable and of high precision in terms of the
436 laboratory methods, cannot be considered as a solid argument to support their
437 model for vein formation.

438

439 **5. Conclusions**

440 Billi et al. (2017) proposed that travertine deposits on horizontal and/or
441 inclined surfaces can subsequently be folded non-tectonically by volume-
442 change processes. Herein, we have shown that: (i) a comparison with active
443 travertine systems and the extensive literature on the topic do not support the
444 interpretations proposed by Billi et al. (2017); (ii) the criteria proposed by Billi
445 et al. (2017) are largely disproved, as most are based on questionable
446 interpretations; (iii) the deformation model proposed by Billi et al. (2017) is not
447 supported by evidence that is available from spring systems found throughout
448 the world. Therefore, we do not recommend using the nine criteria that Billi et
449 al. (2017) proposed to distinguish between primary and secondary travertine
450 structures.

451

452 **Acknowledgements**

453 We are grateful to the Editor and an anonymous reviewer whose comments
454 and suggestions helped us to improve this comment.

455

456

457 **References**

458 Alçiçek, H., Bülbül, A., Alçiçek, M.C., 2016. Hydrogeochemistry of the thermal
459 waters from the Yenice Geothermal Field (Denizli Basin, SW Turkey). *Journal of*
460 *Volcanology and Geothermal Research* 309, 118-138.

461

462 Alçiçek H. Bülbül A. Capezzuoli E. Brogi A. Liotta D. Meccheri M. Riggueri G.
463 Yavuzer İ. Alçiçek M.C. 2017. Origin, evolution and geothermometry of thermal
464 waters in the Gölemezli Geothermal Field, Denizli Basin (SW Turkey). *J*
465 *Volcanol Geotherm Res* doi: 10.1016/j.jvolgeores.2017.07.021

466

467 Alonso-Zarza, A.M., Tanner, L.H. (Eds.) (2010): *Carbonates in Continental*
468 *Settings, Developments in Sedimentology No.61, Elsevier* 378 p.

469

470 Altunel, E., Hancock, P.L., 1993a. Morphology and structural setting of
471 Quaternary travertines at Pamukkale, Turkey', *Geol. J.* 28, 335-346.

472

473 Altunel, E., Hancock, P.L., 1993b. Active Fissuring and Faulting in Quaternary
474 Travertines at Pamukkale, Western Turkey. In: Stewart, I.S., Vita-Finzi, C.,
475 Owen, L.A. (Eds.), *Neotectonics and Active Faulting: Zeitschrift Für*
476 *Geomorphologie Supplement Vol. 94, pp. 285-302.*

477

478 Altunel, E., Karabacak, V., 2005. Determination of horizontal extension from
479 fissure-ridge travertines: a case study from the Denizli Basin, southwestern
480 Turkey. *Geodin. Acta* 18, 333-342.

481

482 Arenas-Abad, C., Vazquez-Urbez, M., Pardo-Tirapu, G., Sancho-Marcen, C.,
483 2010. Fluvial and associated carbonate deposits. Ch.3. in Alonso-Zarza, A.M.
484 and Tanner, L.H. (Eds.): *Carbonates in Continental settings, Developments in*
485 *Sedimentology No.61, Elsevier* 133-175.

486

487 Atabey, E., 2002. The formation of fissure ridge type laminated travertine-tufa
488 deposits microscopical characteristics and diagenesis, Kirşehir, Central
489 Anatolia. *Bulletin of the General Directorate of Mineral Research and*
490 *Exploration of Turkey* 123-124, 59-65.

491

492

493 Bargar, K.E., 1978. Geology and thermal history of Mammoth Hot springs,
494 Yellowstone National Park, Wyoming. *U.S. Geol Surv Bull* 1444, 1-55.

495

496 Bathurst, R.G.C., 1995. Burial diagenesis of limestones under simple
497 overburden. Stylolites, cementation and feedback. *Bull. Soc. Geol. Fr.* 166,
498 181-192.

499 Bertini, A., Minissale, A., Ricci, M., 2008. Use of Quaternary travertine of

500 central-southern Italy as archives of paleoclimate, paleohydrology and
501 neotectonics. *Ital. J. Quatern. Sci.* 21, 99–112.

502

503 Billi, A., Berardi, G., Gratier, J.P., Rossetti, F., Vignaroli, G., Baykara, M.O.,
504 Bernasconi, S.M., Kele, S., Soligo, M., De Filippis, L., Shen, C.C., 2017. First
505 records of syn-diagenetic non-tectonic folding in Quaternary thermogene
506 travertines caused by hydrothermal incremental veining. *Tectonophysics* 700-
507 701, 60-79.

508

509 Bohacs, K.M., Carroll, A.R., Neal, J.E., Mankiewicz, P.Z., 2000. Lake-basin
510 type, source potential, and hydrocarbon character: an integrated sequence-
511 stratigraphic-geochemical framework. In: Gierlowski-Kordesh, E.H., Kerry, K.R.
512 (Eds.), *Lake Basins through Space and Time*. Am. Assoc. Petrol. Geol. Stud.
513 Geol. vol. 46, pp. 3-33.

514 Bonny, S., Jones, B., 2003. Microbes and mineral precipitation, Miette Hot
515 Springs, Jasper National Park, Alberta, Canada. *Canadian Journal of Earth*
516 *Sciences* 40(11), 1483-1500.

517

518 Bons, P.D., Elburg, M. A., Gomez-Rivas, E., 2012. A review of the formation of
519 tectonic veins and their microstructures. *Journal of Structural Geology* 43, 33-
520 62.

521

522 Brogi, A., 2004. Faults linkage, damage rocks and hydrothermal fluid
523 circulation: tectonic interpretation of the Rapolano Terme travertines (southern
524 Tuscany, Italy) in the context of Northern Apennines Neogene–Quaternary
525 extension. *Eclogae Geol. Helvetiae* 97, 307–320.

526

527 Brogi, A., Capezzuoli, E., 2009. Travertine deposition and faulting: the fault-
528 related travertine fissure-ridge at Terme S. Giovanni, Rapolano Terme (Italy).
529 *Int. J. Earth Sci.* 98, 931–947.

530 Brogi, A., Capezzuoli, E., 2014. Earthquake impact on fissure-ridge type
531 travertine deposition. *Geological Magazine* 151, 1135–1143.

532 Brogi, A., Capezzuoli, E., Aquè, R., Branca, M., Voltaggio, M., 2010. Studying
533 travertines for neotectonics investigations: Middle-Late Pleistocene syn-
534 tectonic travertine deposition at Serre di Rapolano (Northern Apennines, Italy).
535 *Int. J. Earth Sci.* 99, 1383–1398.

536

537 Brogi, A., Capezzuoli, E., Buracchi, E., Branca, M., 2012. Tectonic control on
538 traver-tine and calcareous tufa deposition in a low-temperature geothermal
539 system (Sarteano, Central Italy). *J. Geol. Soc. Lond.* 169, 461–476.

540

- 541 Brogi, A., Capezzuoli, E., Alçiçek, M.C., Gandin, A., 2014a. Evolution of a fault-
542 controlled travertine fissure-ridge in the western Anatolia extensional province:
543 the Çukurbağ fissure-ridge (Pamukkale, Turkey). *J. Geol. Soc. Lond.* 171, 425-
544 441.
- 545
- 546 Brogi, A., Capezzuoli, E., Martini, I., Picozzi, M., Sandrelli, F., 2014b. Late
547 Quaternary tectonics in the inner Northern Apennines (Siena Basin, southern
548 Tuscany, Italy) and their seismotectonic implication. *J. Geodyn.* 76, 25-45.
- 549
- 550 Brogi, A., Alçiçek, C., Yalçiner, C. C., Capezzuoli, E., Liotta, D., Meccheri, M.,
551 Rimondi, V., Ruggieri, G., Gandin, A., Boschi, C., Büyüksara, A., Alçiçek, H.,
552 Bülbül, A., Baykara, M.O., Shen, C-C., 2016. Hydrothermal fluids circulation
553 and travertine deposition in an active tectonic setting: insights from the
554 Kamara geothermal area (western Anatolia, Turkey). *Tectonophysics* 680,
555 211-232.
- 556
- 557 Brogi, A., Capezzuoli, E., Kele, S., Baykara, M.O., Shen, C.C. 2017. Key
558 travertine tectofacies for neotectonics and palaeoseismicity reconstruction:
559 effects of hydrothermal overpressured fluid injection. *Journal of the Journal of*
560 *the Geological Society*. <https://doi.org/10.1144/jgs2016-124>
- 561 Çakır, Z., 1999. Along-strike discontinuity of active normal faults and its
562 influence on quaternary travertine deposition: examples from western Turkey.
563 *Turk. J. Earth Sci.* 8, 67-80.
- 564 Capezzuoli, E., Gandin, A., Pedley, M., 2014. Decoding tufa and travertine
565 (fresh water carbonates) in the sedimentary record: the state of the art.
566 *Sedimentology* 61, 1-21.
- 567 Carrara, C., Ciuffarella, L., Paganin, G., 1998. Inquadramento geomorfologico
568 e climatico ambientale dei travertini di Rapolano Terme (SI). *Italian Journal of*
569 *Quaternary Sciences* 11, 319-329.
- 570 Carroll, A.R., Bohacs, K.M., 1999. Stratigraphic classification of ancient lakes:
571 balancing tectonic and climatic controls. *Geology* 27, 99-102.
- 572 Chafetz, H.S., Folk, R.L., 1984. Travertines: depositional morphology and the
573 bacterially constructed constituents. *J. Sediment. Petrol.* 54, 289-316.
- 574
- 575 Chafetz, H.S., Guidry, S.A., 1999. Bacterial shrubs, crystal shrubs, and ray-
576 crystal shrubs: bacterial vs. abiotic precipitation. *Sediment. Geol.* 126, 57-74.
- 577
- 578 Chafetz, H.S., Rush, P.R., Utech, N.M., 1991. Microenvironmental controls on
579 mineralogy and habit of CaCO₃ precipitates: an example from active travertine

580 system. *Sedimentology* 38, 107-126.

581

582 Claes, H., Soete, J., Van Noten, K., El Desouky, H., Marques Erthal, M.,
583 Vanhaecke, F., Ozkul, M., Swennen, R., 2015. *Sedimentology*, three-
584 dimensional geobody reconstruction and carbon dioxide origin of Pleistocene
585 travertine deposits in the Ballik area (south-west Turkey). *Sedimentology* 62,
586 1408-1445.

587

588 Claes, H., Degros, M., Soete, J., Claes, S., Kele, S., Mindszenty, A., Török, Á.,
589 El Desouky, H., Vanhaecke, F., Swennen, R., 2017. Geobody architecture,
590 genesis and petrophysical characteristics of the Budakalasz travertines, Buda
591 Hills (Hungary). *Quaternary International* (2016),
592 <http://dx.doi.org/10.1016/j.quaint.2016.09.007>

593 Croci, A., Della Porta, G., Capezzuoli, E., 2016. Depositional architecture of a
594 mixed travertine-terrigenous system in a fault-controlled continental
595 extensional basin (Messinian, Southern Tuscany, Central Italy). *Sedimentary*
596 *Geology* 332, 13-39.

597

598 D'Argenio, B., Ferreri, M., Ferreri, V., Stanzione, D., 1981. Travertines of
599 Southern Italy. Texture, Geochemistry and Sedimentary Model. IAS 2nd
600 Eur.Meeting, Abstracts, 43-44.

601

602 D'Argenio, B., Ferreri, V., 1987. A brief outline of sedimentary models for
603 Pleistocene travertine accumulation in Southern Italy. *Rend. Soc. Geol. It.* 9 –
604 167-170.

605

606 D'Argenio, B., Ferreri, V., 1988. Ambienti di deposizione e litofacies dei
607 travertini Quaternari dell'Italia Centro-Meridionale. *Mem. Soc. Geol. It.* 41,
608 861-868.

609

610 D'Argenio, B., Violante, C., Golubic, S., 1995. Travertines as proxies to
611 climate-controlled/controlling carbonates in geologic time. An Introduction. In:
612 Della Porta, G., 2015. Carbonate build-ups in lacustrine, hydrothermal and
613 fluvial settings: comparing depositional geometry, fabric types and
614 geochemical signature In: Bosence, D. W. J., Gibbons, K. A., Le Heron, D. P.,
615 Morgan, W. A., Pritchard, T. & Vining, B. A. (eds), *Microbial Carbonates in*
616 *Space and Time: Implications for Global Exploration and Production*. Geological
617 Society, London, Special Publications 418, 17-68.

618

619 Della Porta, G., Capezzuoli, E., De Bernardo, A., 2017. Facies character and
620 depositional architecture of hydrothermal travertine slope aprons (Pleistocene,
621 Acquasanta Terme, Central Italy), *Marine and Petroleum Geology* (2017),

622 <http://dx.doi.org/10.1016/j.marpetgeo.2017.03.014>.

623

624 Ubertini, L., Castelli, F., Bras, R.L. (eds.): Climate change and hydrological
625 hazards in the Mediterranean area. Nat.Res.Council of Italy, Perugia, 17-23.

626

627 Erthal, M.M., Capezzuoli, E., Mancini, A., Claes, H., Soete, J., Swennen, R.,
628 2017. Shrub morpho-types as indicator for the water flow energy – Tivoli
629 travertine case (central Italy). *Sediment. Geology* 347, 79-99.

630

631 Faccenna, C., Soligo, M., Billi, A., De Filippis, L., Funiciello, R., Rossetti, C.,
632 Tuccimei, P., 2008. Late Pleistocene depositional cycles of the Lapis Tiburtinus
633 travertine (Tivoli, Central Italy): possible influence of climate and fault activity.
634 *Global Planet. Change* 63, 299–308.

635

636 Flügel, E., 2004. *Microfacies of carbonate rocks. Analysis, interpretation and*
637 *application*. Springer (New York). 976 pp.

638

639 Folk, R.L., Chafetz, H.S., Tiezzi, P.A., 1985. Bizarre forms of the depositional
640 and diagenetic calcite in hot spring travertines, Central Italy. In:
641 Schneidermann, N., Harris, P.M. (Eds.) *Carbonate Cements*, Soc. Econ.
642 *Paleont. Miner. Spec. Publ.* 36, 349–369.

643

644 Folk, R.L., 1994. Interaction between bacteria, nannobacteria and mineral
645 precipitation in hot springs of Central Italy. *Geogr. Phys. Quatern.* 48, 233-
646 246.

647

648 Ford, T.D., Pedley, H.M., 1996. A review of tufa and travertine deposits of the
649 world. *Earth Sci. Rev.* 41, 117-175.

650

651 Ford, D., Williams, P., 2007. *Karst Hydrogeology and Geomorphology*. pp. 562.
652 John Wiley & Sons Ltd

653

654 Fouke, B.W., Farmer, J.D., Des Marais, D.J., Pratt, L., Sturchio, N.C., Burns,
655 P.C., Discipulo, M.K., 2000. Depositional facies and aqueous-solid
656 geochemistry of travertine depositing hot springs (Angel Terrace, Mammoth
657 Hot Springs, Yellowstone National Park, USA). *J. Sediment. Res.* 70, 265-285.

658

659 Fouke, B.W., Bonheyo, G.T., Sanzenbacher, B., Frias-Lopez, J., 2003.
660 Partitioning of bacterial communities between travertine depositional facies at
661 Mammoth Hot Springs, Yellowstone National Park, USA. *Canadian Journal of*
662 *Earth Sciences* 40, 1531-1548.

663

664 Frery, E., Gratier, J.P., Ellouz-Zimmerman, N., Deschamps, P., Blamart, D.,

665 Hamelin, B., Swennen, R., 2016. Geochemical transect through a travertine
666 mount: A detailed record of CO₂-enriched fluid leakage from Late Pleistocene
667 to present-day Little Grand Wash fault (Utah, USA), *Quaternary International*
668 (2016), <http://dx.doi.org/10.1016/j.quaint.2016.09.035>
669

670 Gandin, A., Wright, D.T., 2007. Evidence of vanished evaporites in
671 Neoproterozoic carbonates of South Africa. In: Schreiber, B.C., Lugli, S., Babel,
672 M. (Eds.). *Evaporites through space and time*. Geological Society, London,
673 Special Publications 285, 285-308. ISBN 978-1-86239-232-8
674

675 Gandin, A., 2013 *Classificazione genetica, caratteri petrologici distintivi e valori*
676 *isotopici correlati di calcari incrostanti depositi da acque scorrenti (Travertini -*
677 *Calcareous Tufa - Speleotemi)*. *Rend. Online Soc. Geol. It.* 27, 10-30.
678

679 Gandin, A., Capezzuoli, E., 2014. Travertine: distinctive depositional fabrics of
680 carbonates from thermal spring systems. *Sedimentology* 61, 264–290.
681

682 Geurts, M.-A., Frappier, M., Tsien, H.H., 1992. Morphogenèse des barrages de
683 travertin de Coal Springs, Sud-est du territoire du Yukon, *Géogr. phys. et*
684 *Quaternaire* 46, 221–232.
685

686 Goldenfeld, N., Chan, P.Y., Veysey, J., 2006. Dynamics of precipitation pattern
687 formation at geothermal hot springs. *Phys. Rev. Lett.* 96, 254501-1–254501-4.
688

689 Gradzinski, M., Wroblewski, W., Dulinski, M. & Hercman, H., 2014.
690 Earthquake- affected development of a travertine ridge. *Sedimentology* 61,
691 238–263.
692

693 Gratier, J.P., Frery, E., Deschamps, P., Røyne, A., Renard, F., Dysthe, D.,
694 Ellouz-Zimmerman, N., Hamelin, B., 2012. How travertine veins grow from top
695 to bottom and lift the rocks above them: the effect of crystallization force.
696 *Geology* 40, 1015–1018.

697 Guo, L., Riding, R., 1992. Micritic aragonite laminae in hot water travertine
698 crust, Rapolano Terme. *Sedimentology* 39, 1067–1079.
699

700 Guo, L., Riding, R., 1994. Origin and diagenesis of Quaternary travertine shrub
701 fabrics, Rapolano Terme, Central Italy. *Sedimentology* 41, 499–520.
702

703 Guo, L., Riding, R., 1998. Hot-spring travertine facies and sequences, late
704 Pleistocene, Rapolano Terme, Italy. *Sedimentology* 45, 163–180.
705

706 Guo, L., Riding, R., 1999. Rapid facies changes in Holocene fissure ridge hot

- 707 spring travertines, Rapolano Terme, Italy. *Sedimentology* 46, 1145–1158.
708
- 709 Guo, L., Andrews, J., Riding, R., Dennis, P., Dresser, Q., 1996. Possible
710 microbial effects on stable carbon isotopes in hot-springs travertines. *Journal*
711 *of Sedimentary Research* 66, 468–473.
- 712 Hammer, Ø., Dysthe, D.K., Jamtveit, B., 2007. The dynamics of travertine
713 dams. *Earth Planet. Sci. Lett.* 256, 258–263.
714
- 715 Hammer, Ø., Dysthe, D.K., Jamtveit, B., 2010. Travertine terracing: patterns
716 and mechanisms. In: Pedley, M., Rogerson, M. (Eds.). *Tufas, Speleothems*
717 *and Stromatolites: Unravelling the Physical and Microbial Controls*, Geological
718 Society, London, Special Publications 336, 345–355.
719
- 720 Hammer, Ø., Jamtveit, B., Benning, L., Dysthe, D. K., 2005. Evolution of fluid
721 chemistry during travertine formation in the Troll thermal springs, Svalbard,
722 Norway. *Geofluids* 5, 140–150.
723
- 724 Hancock, P.L., Chalmers, R.M.L., Altunel, E., Çakır, Z., 1999. Travertines: using
725 travertines in active fault studies. *J. Struct. Geol.* 21, 903–916.
726
- 727 Heap, M.J., Baud, P., Reuschle, T., Meredith, P.G., 2014. Stylolites in
728 limestones: barriers to fluid flow? *Geology* 42, 51–54.
- 729 Henchiri, M., Ahmed, W.B., Brogi, A., Alçiçek, M.C., Benassi, R., 2017.
730 Evolution of Pleistocene travertine depositional system from terraced slope to
731 fissure-ridge in a mixed travertine-alluvial succession (Jebel El Mida, Gafsa,
732 southern Tunisia). *Geodinamica Acta*, 29/1, 20–41.
733
- 734 Jones, B., Renaut, R.W., 1995. Noncrystallographic dendrites from hot-spring
735 deposits at Lake Bogoria, Kenya. *Journal of Sedimentary Research* 65,
736 1542–169.
737
- 738 Jones, B., Renaut, R.W., 2008. Cyclic development of large, complex, calcite
739 dendrite crystals in the Clinton travertine, Interior British Columbia, Canada.
740 *Sediment. Geol.* 203, 17–35.
741
- 742 Jones, B., Renaut, R.W., 2010. Calcareous spring deposits in continental
743 settings. In: Ed Alonso-Zarza A.M. & Tanner L.H. "Carbonates in continental
744 settings". *Developments in Sedimentology* 61, 177–224.
745
- 746 Jones, B., Renaut, R.W., 1996. Influence of thermophilic bacteria on calcite
747 and silica precipitation in hot springs with water temperatures above 90°C:
748 evidence from Kenya and New Zealand. *Canadian Journal of Earth Sciences* 33,

749 72-83.

750

751 Jones, B., Renaut, R.W., Owen, R.B., Torfason, H., 2005. Growth patterns and
752 implications of complex dendrites in calcite travertines from Lysuholl,
753 Snæfellsnes, Iceland. *Sedimentology* 52, 1277-1301.

754

755 Jones, B., Renaut, R.W., Rosen, M.R., 2000. Trigonal dendritic calcite crystals
756 forming from hot spring waters at Waikite, North Island, New Zealand. *Journal*
757 *of Sedimentary Research* 70, 586-603.

758

759 Kele, S., Demény, A., Siklósy, Z., Németh, T., Tóth, M., Kovács, M., 2008.
760 Chemical and stable isotope composition of recent hot-water travertines and
761 associated thermal waters from Egerszalók, Hungary: Depositional facies and
762 non-equilibrium fractionation. *Sed. Geo.* 211, 53-72.

763

764 Koehn, D., Rood, M.P., Beaudoin, N., Chung, P., Bons, P.D., Gomez-Rivas, E.
765 2016. A new stylolite classification scheme to estimate compaction and local
766 permeability variations. *Sedimentary Geology* 346, 60-71.

767

768 Khatib, S., Rochette, P., Alçiçek, M.C., Lebatard, A.-E., Demory, F., Saos, T.,
769 2014. Etude stratigraphique, sédimentologique et paléomagnétique des
770 travertins de Denizli (Turquie) contenant des restes fossiles quaternaires
771 (Stratigraphic, sedimentological and paleomagnetic study of the Kocabaş
772 travertines, Denizli Basin, Anatolia, Turkey). *Anthropologie* 118, 16-33.

773

774 Ku, T.L., Liang, Z.L., 1985. The dating of impure carbonates with decay- series
775 isotopes. *Nucl. Instrum. Methods Phys. Res.* 223, 563-571. doi:10.1016/0167-
776 5087(84)90710-5.

777 Lebatard A.-E. Alçiçek M.C. Rochette P. Khatib S. Vialet A. Boulbes N.
778 Bourlès D.L. Demory F. Guipert G. Mayda S. Titov V.V. Vidal L. de Lumley H.
779 2014. Dating the Homo erectus bearing travertine from Kocabaş (Denizli,
780 Turkey) at at least 1.1 Ma. *Earth and Planetary Science Letters* 390, 8-18.

781

782 Liu, Z., Svensson, U., Dreybrodt, W., Daoxian, Y., Buhmann, D., 1995.
783 Hydrodynamic control of inorganic precipitation in Huanglong Ravine, China:
784 field measurements and theoretical prediction of deposition rates. *Geochim.*
785 *Cosmochim. Acta* 59, 3087-3097.

786

787 Lu, G., Zheng, C., Donahoe, R.J., Lyons, W.B., 2000. Controlling processes in a
788 CaCO₃ precipitating stream in Huanglong Natural Scenic District, Sichuan,
789 China. *J. Hydrol.* 230, 34-54.

790

791 Mesci, B.L., Gursoy, H., Tatar, O., 2008. The evolution of travertine masses in

792 the Sivas Area (Central Turkey) and their relationships to active tectonics.
793 Turk. J. Earth Sci. 17, 219–240.

794

795 Navarro, A., Font, X., Viladevall, M., 2011. Geochemistry and groundwater
796 contamination in the La Selva geothermal system (Girona, Northeast Spain).
797 Geothermics 40, 275–285.

798

799 Pasvanoglu, S., Chandrasekharam, D., 2011. Hydrogeochemical and isotopic
800 study of thermal and mineralized waters from the Nevsehir (Kozakli) area,
801 Central Turkey. J. Volcanol. Geoth. Res. 202, 241–250.

802

803 Pedley, H.M., 1990. Classification and environmental models of cool freshwater
804 tufas. Sediment. Geol. 68, 143-154.

805

806 Pedley, H.M., 2009. Tufas and travertines of the Mediterranean region: a
807 testing ground for freshwater carbonate concepts and developments.
808 Sedimentology 56, 221-246

809

810 Pentecost, A., 1995. The quaternary travertine deposits of Europe and Asia
811 minor. Quat. Sci. Rev. 14, 1005-1028.

812

813 Pentecost, A., 2005. Travertine. Springer, Berlin, p. 445.

814

815 Pola, M., Gandin, A., Tuccimei, P., Soligo, M., Deiana, R., Fabbri, P., Zampieri,
816 D., 2014. A multidisciplinary approach to understanding carbonate deposition
817 under tectonically controlled hydrothermal circulation: A case study from a
818 recent travertine mound in the Euganean hydrothermal system, northern Italy.
819 Sedimentology 61, 172-199.

820

821 Rainey, D.K., Jones, B., 2009. Abiotic versus biotic controls on the
822 development of the Fairmont Hot Springs carbonate deposit, British Columbia,
823 Canada. Sedimentology 56, 1832–1857.

824

825 Ricci, M., Bertini, A., Capezzuoli, E., Horvatinčić, N., Andrews, J.E., Fauquette,
826 S., Fedi, M., 2015. Palynological investigation of a Late Quaternary calcareous
827 tufa and travertine deposit: A case study of Bagnoli in the Valdelsa Basin
828 (Tuscany, central Italy). Review of Palaeobotany and Palynology 218, 184-197.

829

830 Riding, R., 1991. Classification of microbial carbonates. - In: Riding, R. (ed.):
831 Calcareous algae and stromatolites 21-51, Berlin (Springer).

832

833 Rihs, S., Condomines, M., Poidevin, J.L., 2000. Longterm behaviour of
834 continental hydrothermal systems: Useries study of hydrothermal carbonates

835 from the French Massif Central (Allier Valley). *Geochim. Cosmochim. Acta* 418,
836 3189–3199.

837

838 Rimondi, V., Costagliola, P., Ruggieri, G., Benvenuti, M., Boschi, C., Brogi, A.,
839 Capezzuoli, E., Morelli, G., Gasparon, M., Liotta, D., 2016. Investigating fossil
840 hydrothermal systems by means of fluid inclusions and stable isotopes in
841 banded travertine: an example from Castelnuovo dell'Abate (southern
842 Tuscany, Italy). *Int. J. Earth Sci.* 105 (22), 659–679.
843 <http://dx.doi.org/10.1007/s00531-015-1186-y>.

844 Rogerson, H.M., Pedley, M., Kelham, A., Wadhawan, J.D., 2014. Linking
845 mineralisation process and sedimentary product in terrestrial carbonates using
846 a solution thermodynamic approach. *Earth Surface Dynamics* 2: p. 197-216.

847

848 Rolland, A., Toussaint, R., Baud, P., Schmittbuhl, J., Conil, N., Koehn, D.,
849 Renard, F., Gratier, J.-P., 2012. Modeling the growth of stylolites in
850 sedimentary rocks. *J. Geophys. Res. Solid Earth* 117, B06403.

851

852 Ronchi, P., Cruciani, F., 2015. Continental carbonates as a hydrocarbon
853 reservoir, an analog case study from the travertine of Saturnia, Italy. *AAPG*
854 *Bulletin* 99(4), 711-734.

855

856 Rutter, E.H., 1972. The influence of interstitial water on the rheological
857 behaviour of calcite rocks. *Tectonophysics* 14, 13-33.

858

859 Scheuer, G., Schweitzer, F., 1981. Origin of the freshwater limestones of
860 Hungary and comparative studies, *Föld. Közl.* 111, 67–97.

861

862 Schlanger, 1964, In: Sadd, J., Alsharhan. A. 2000. Stylolites in lower
863 cretaceous carbonate reservoir, U.A.E. *SEPM Special publication*, No. 69, pp
864 185-207.

865

866 Schreiber, B.C., Smith, D., Schreiber, E., 1981. Spring peas from New York
867 State: nucleation and growth of fresh water hollow oolites and pisolites. *J.*
868 *Sed. Petrol.* 50, 1341–1346.

869

870 Selçuk, A.S., Erturaç, M.K., Üner, S., Özsayın, E., Pons-Branchu, E., 2017.
871 Evolution of Çamlık fissure-ridge travertines in the Baskale basin (Van, Eastern
872 Anatolia), *Geodinamica Acta* 29/1, 1-19.

873

874 Sellier, 1979, In: Sadd, J., Alsharhan. A. 2000. Stylolites in lower cretaceous
875 carbonate reservoir, U.A.E. *SEPM Special publication*, No. 69, pp 185-207.

876

- 877 Sierralta, M., Kele, S., Melcher, F., Hambach, U., Reinders, J., van Geldern, R.,
878 Frechen, M., 2010. Uranium-series dating of travertine from Sutto:
879 implications for reconstruction of environmental change in Hungary. *Quatern.*
880 *Int.* 222, 178–193.
- 881
- 882 Soligo, M., Tuccimei, P., Barberi, R., Delitata, M.C., Miccadei, E., Taddeucci, A.,
883 2002. U/Th dating of freshwater travertine from middle Velino Valley (Central
884 Italy): paleoclimatic and geological implications. *Palaeogeogr. Palaeoclimatol.*
885 *Palaeoecol.* 184, 147–161.
- 886
- 887 Sturchio, N.P., Pierce, K.L., Murrel, M.T., Sorey, M.L., 1994. Uranium series
888 ages of travertines and timing of the Last Glaciation in the Northern
889 Yellowstone Area, Wyoming Montana. *Quatern. Res.* 41, 265–277.
- 890
- 891 Taylor, S.R., McLennan, S.M., 1995. The geochemical evolution of the
892 continental crust. *Reviews in Geophysics* 33, 241–265.
- 893
- 894 Temiz, U., Eikenberg, J., 2011. U/Th dating of the travertine deposited at
895 transfer zone between two normal faults and their neotectonic significance:
896 Cambazli fissure ridge travertines (the Gediz Graben - Turkey). *Geodinamica*
897 *Acta* 24, 95-105.
- 898
- 899 Temiz, U., Gökten, Y.E., Eikenberg, J., 2013. Strike-slip deformation and U/Th
900 dating of travertine deposition: Examples from North Anatolian Fault Zone,
901 Bolu and Yeniçağ Basins, Turkey. *Quaternary International* 12, 132-140.
- 902
- 903 Temiz, U., Gökten., E, Eikenberg, J., 2009. U/Th dating of fissure ridge
904 travertines from the Kirsehir region (Central Anatolia Turkey): structural
905 relations and implications for the Neotectonic development of the Anatolian
906 block. *Geodinamica Acta* 22, 201-213.
- 907
- 908 Török, Á., Mindszenty, A., Claes, H., Kele, S., Fodor, L., Swennen, R., 2017.
909 Geobody architecture of continental carbonates: "Gazda" travertine quarry
910 (Süttő, Gerecse Hills, Hungary), *Quat. Int.*, 1-22.
- 911 Tucker., M., 1988. *Sedimentary Petrology. An Introduction.* Blackwell Scientific
912 Publication, 252 p.
- 913 Uysal, I.T., Feng, Y., Zhao, J.X., Altunel, E., Weatherley, D., Karabacak, V.,
914 Cengiz, O., Golding, S.D., Lawrence, M.G., Collerson, K.D., 2007. U-series
915 dating and geochemical tracing of late Quaternary travertine in co-seismic
916 fissures. *Earth Planet. Sci. Lett.* 257, 450–462.
- 917 Uysal, I.T., Feng, Y., Zhao, J., Isik, V., Nuriel, P., Golding, S., 2009.

- 918 Hydrothermal CO₂ degassing in seismically active zones during the late
919 Quaternary. *Chem. Geol.* 265, 442–454.
- 920 Uysal, I.T., Feng, Y., Zhao, J., Bolhar, R., Isik, V., Baublys, K.A., Yago, A.,
921 Golding, S.D., 2011. Seismic cycles recorded in late Quaternary calcite veins:
922 geochronological, geochem- ical and microstructural evidence. *Earth Planet.*
923 *Sci. Lett.* 303, 84–96.
- 924 Veysey, J., Goldenfeld, N. 2008. Watching rocks grow, 4, 310–313.
- 925
- 926 Violante, C., D’Argenio, B., Ferreri, V., Golubic, S., 1994a. Sedimentary Model
927 of Quaternary Travertine deposits. Abstracts, IAS 15th Reg.Meeting, Ischia
928 (Italy), 426-428.
- 929
- 930 Violante, C., Ferreri, V., D’Argenio, B., Golubic, S., 1994b. Quaternary
931 Travertines at Rochetta a Volturmo (Isernia, Central Italy). Facies Analysis and
932 Sedimentary Model of an Organogenic Carbonate System. Excursion A1, in:
933 Pre-Meeting Fieldtrip Guidebook, IAS 15th Reg.Meeting, Ischia (Italy), 5-23.
- 934
- 935 Walker, M. 2005. Quaternary dating methods. Wiley (England)
- 936
- 937 Warren, J.K., 1999. Evaporites: their evolution and economics. Blackwell
938 Scientific, Oxford, UK. 438 p.
- 939 Warren, J.K., 2006. Evaporites: Sediments, Resources and Hydrocarbons.
940 Springer, Berlin. 1036 p.
- 941 Warwick, G.T., 1952. Rimstone pools and associated phenomena. *Trans Cave*
942 *Res Group GB* 2, 153–165.
- 943
- 944 Shipton, Z.K., Evans, J.P., Dockrill, B., Heath, J., Williams, A., Kirchner, D.,
945 Kolesar, P.T., 2005. Natural leaking CO₂-charged systems as analogs for failed
946 geologic storage reservoirs, in: D. Thomas (Ed.), *Carbon Dioxide Capture for*
947 *Storage in Deep Geologic Formations -Results from the CO₂ Capture Project* vol.
948 2, Elsevier Science (2005), pp. 699–712.
- 949
- 950 Zentmyer, R., Myrow, P.M., Newell, D.L., 2008. Travertine deposits from along
951 the South Tibetan Fault System near Nyalam, Tibet. *Geol. Mag.* 145, 753–765.
- 952
- 953
- 954
- 955

956 **Figure Captions**

957

958 Fig. 1 – a) Terraced depositional system at Saturnia (Italy) with pools and

959 rims, where calcite crystallize as a result of CO₂ degassing from flowing
960 carbonate-rich thermal waters; b) example of crystalline layers
961 (crystalline crusts) deposited on the slope system and formed by dendritic
962 calcite crystals; c) detail of the crystalline crusts indicated in (b). d-e)
963 Example of a slope microterraced deposit formed by dendritic calcite
964 crystals forming crystalline crusts (the so-called "chimney-like veins" by
965 Billi et al., 2017); e-f) details of the inset in (e): note the different shape
966 of the crystal-fans along the same level, emphasizing that that the
967 direction of the calcite crystal growth cannot be based on the fan-like
968 crystal arrangements as proposed by Billi et al. (2017).

969

970

971 Fig. 2 - Present-day depositional systems and related macro-facies. a)
972 Terraced slope depositional system at Pamukkale (Turkey); b) Terraced
973 slope depositional system at Karahayıt (Turkey); note the stepped
974 morphology of the terraced slope with metre-scale pools separated by
975 round rims at the pool margin and vertical walls. c-d) Detail of a pool
976 (indicated in b) illustrating the site of precipitation of travertine with
977 different fabrics, such as shrubs, radial pisoids and coated gas bubbles (cf
978 Guo and Riding, 1998); e) micro-terraced slope system; f) detail of micro-
979 terraces showing pools and rims, where the rims are built by crystalline
980 dendrites and pools are sites of precipitation of different travertine fabrics
981 such as shrubs and porous travertine (e.g. coated gas bubbles).

982

983 Fig. 3 - Examples of banded calcite veins filling cracks that cut across layers or
984 follow bedding surfaces; a) banded calcite vein crossing late Pleistocene
985 travertine layers at Bagno Vignoni (southern Tuscany, Italy); b) banded
986 calcite veins system crossing a Pleistocene fissure ridge-type travertine
987 deposit (Akköy fissure-ridge) in the Denizli Basin (Turkey; c) banded
988 calcite vein filling a sub-vertical fracture in the wall of the Akköy fissure
989 ridge from Denizli Basin (Turkey); d) detail of the inset indicated in (b); e)
990 banded calcite veins system filling sub-vertical fractures crossing the
991 middle Pleistocene fissure ridge-type travertine deposit (Çukurbağ fissure-
992 ridge) in the Denizli Basin (Turkey; f) detail of the inset indicated in (e);
993 g) sub-horizontal banded calcite vein filling a fracture sub-parallel to the
994 bedding surfaces in the late Pleistocene-Holocene travertine deposits at
995 Cava Campo Muri (Rapolano Terme, Italy); h) Sub-horizontal and low-
996 angle banded calcite veins system filling a fracture that cut across layers
997 or follow bedding surfaces in the late-Pleistocene-Holocene travertine
998 deposits at Cava Campo Muri (Rapolano Terme, Italy); i) detail of the
999 inset indicated in (h).

1000

1001 Fig. 4 - Photomicrographs of microfabrics of crystalline crusts and banded
1002 calcite veins filling fractures cutting across travertine beds. a-b) example
1003 of crystalline crust from Rapolano Terme (Italy); c-d) example of banded
1004 calcite vein from the Denizli Basin (Turkey). Please note fabric, dimension
1005 and crystal morphology that are different from the interpreted veins by
1006 Billi et al. (2017). Many other examples of micro-fabrics are illustrated in
1007 numerous publications (Gandin and Capezzuoli, 2014; Della Porta, 2015;
1008 Croci et al., 2016; Della Porta et al., 2017 and references therein) to
1009 which the readers are addressed for more details.
1010

1011 Fig. 5 - Photographs of saw-cut walls exposed in the Pianetti quarry near
1012 Saturnia (southern Tuscany, Italy), the same outcrops reported in Billi et
1013 al. 2017. a-b) Slope deposit formed by crystalline crusts giving rise to
1014 terraces in a prograding pools system (the so-called "chimney-like veins"
1015 by Billi et al. 2017, enlarged in c) and the final slope accumulation. The
1016 slope deposit is unconformably overlain by subhorizontal porous strata
1017 formed by shrub facies (typical of subhorizontal pools) terminating in
1018 onlap against the slope depositional profile. c) Decimeter-scale pools and
1019 rims characterized by prograding and aggrading different fabric types. d)
1020 Cross-section of a progradational terraced slope with pools bordered by
1021 round rims prograding and aggrading. The terraced system is
1022 unconformably overlain by subhorizontal strata onlapping against the pool
1023 rims: this geometric configuration is a primary depositional feature and
1024 should not be explained as a secondary features (i.e. the result of syn-
1025 diagenetic folds caused by laterally-confined volume expansion through
1026 hydrothermal incremental veining) as proposed by Billi et al. (2017)
1027 because the subhorizontal porous strata in onlap do not appear deformed
1028 by the alleged syn-diagenetic folding.
1029

1030 Fig. 6 – a) Irregular geometrical setting of travertine beds visible in saw-cut
1031 walls exposed in the Pianetti quarry near Saturnia (southern Tuscany,
1032 Italy), and interpreted by Billi et al. (2017) as the result of refold
1033 structures (cf their Fig. S10); b) Example of an active cascade travertine
1034 depositional system at Bagni San Filippo (southern Tuscany, Italy), where
1035 the sub-vertical slopes explain the geometrical setting of the travertine
1036 beds illustrated in (a) and interpreted by Billi et al. (2017) as secondary
1037 fold structures (i.e. refolded structures). c) Cross-section of a terraced
1038 slope; d) saw-tooth shape of travertine layers deriving from an orthogonal
1039 cross-section of the terraced slope: the saw-tooth shape is the result of
1040 the progradational growth of the microterraced slope.

Figure 1
[Click here to download high resolution image](#)



Fig. 1 – a) Terraced depositional system at Saturnia (Italy) with pools and rims, where calcite crystallize as a result of CO₂ degassing from flowing carbonate-rich thermal waters; b) example of crystalline layers (crystalline crusts) deposited on the slope system and formed by dendritic calcite crystals; c) detail of the crystalline crusts indicated in (b). d-e) Example of a slope microterraced deposit formed by dendritic calcite crystals forming crystalline crusts (the so-called “chimney-like veins” by Billi et al., 2017); e-f) details of the inset in (e): note the different shape of the crystal-fans along the same level reinforcing the fact that the direction of the calcite crystal growth cannot be based on the fans-like crystal arrangement as proposed by Billi et al. (2017).

Figure 2
[Click here to download high resolution image](#)

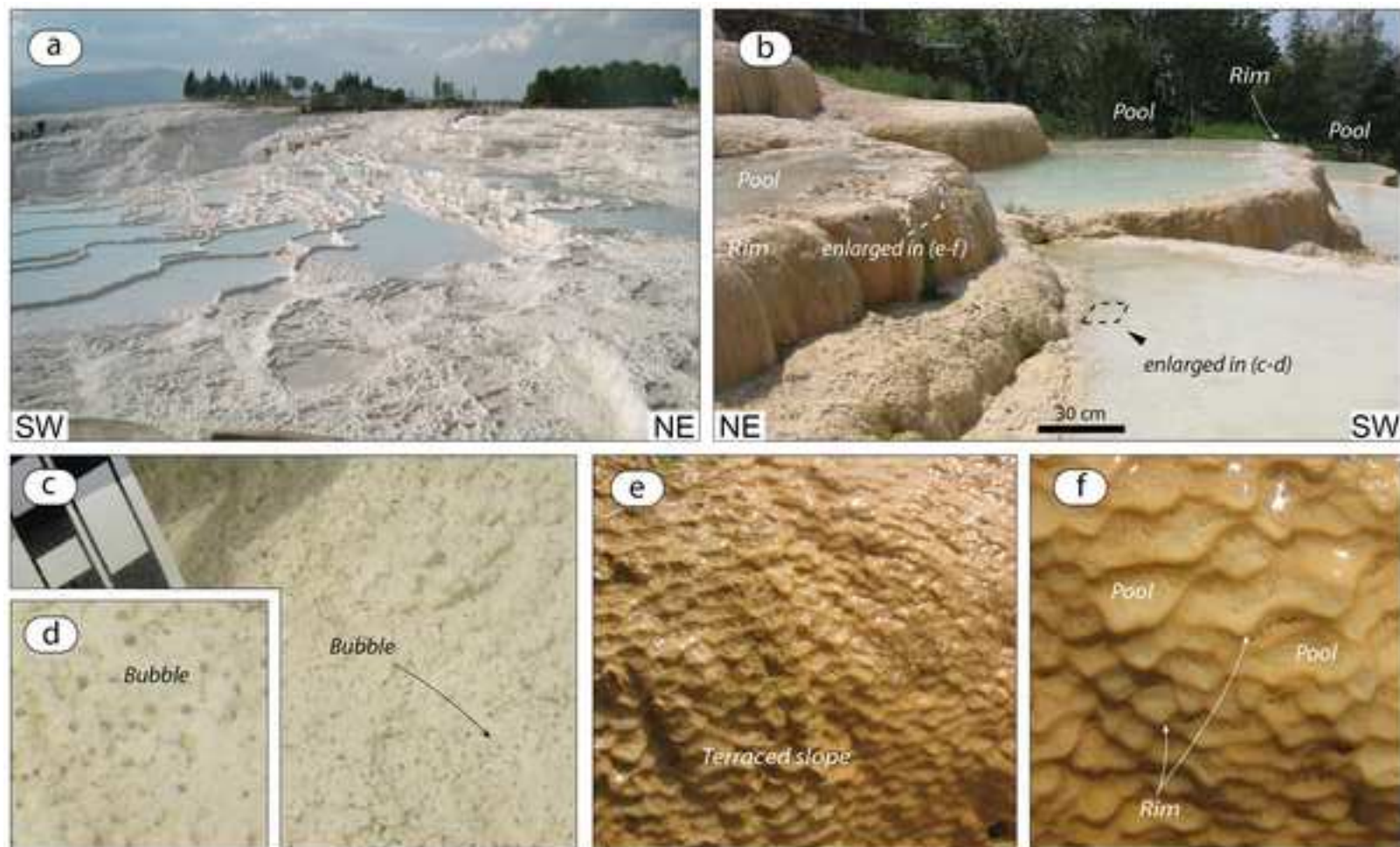


Fig. 2 - Present-day depositional systems and related macrofacies. a) Terraced slope depositional system at Pamukkale (Turkey); b) Terraced slope depositional system at Karahayit (Turkey); note the stepped morphology of the terraced slope with metre-scale pools separated by rounded rim at the pool margin, and vertical walls. c-d) Detail of a pool (indicated in b) illustrating the site of precipitation of travertine with different fabrics, such as shrubs, radial pisoids and coated gas bubbles (cf Guo and Riding, 1998); e) microterraced slope system; f) detail of microterraces showing pools and rims, where the rims are built by crystalline dendrites and pools are sites of precipitation of different travertine fabrics such as shrubs and porous travertine (e.g. coated gas bubbles).

Figure 3
[Click here to download high resolution image](#)

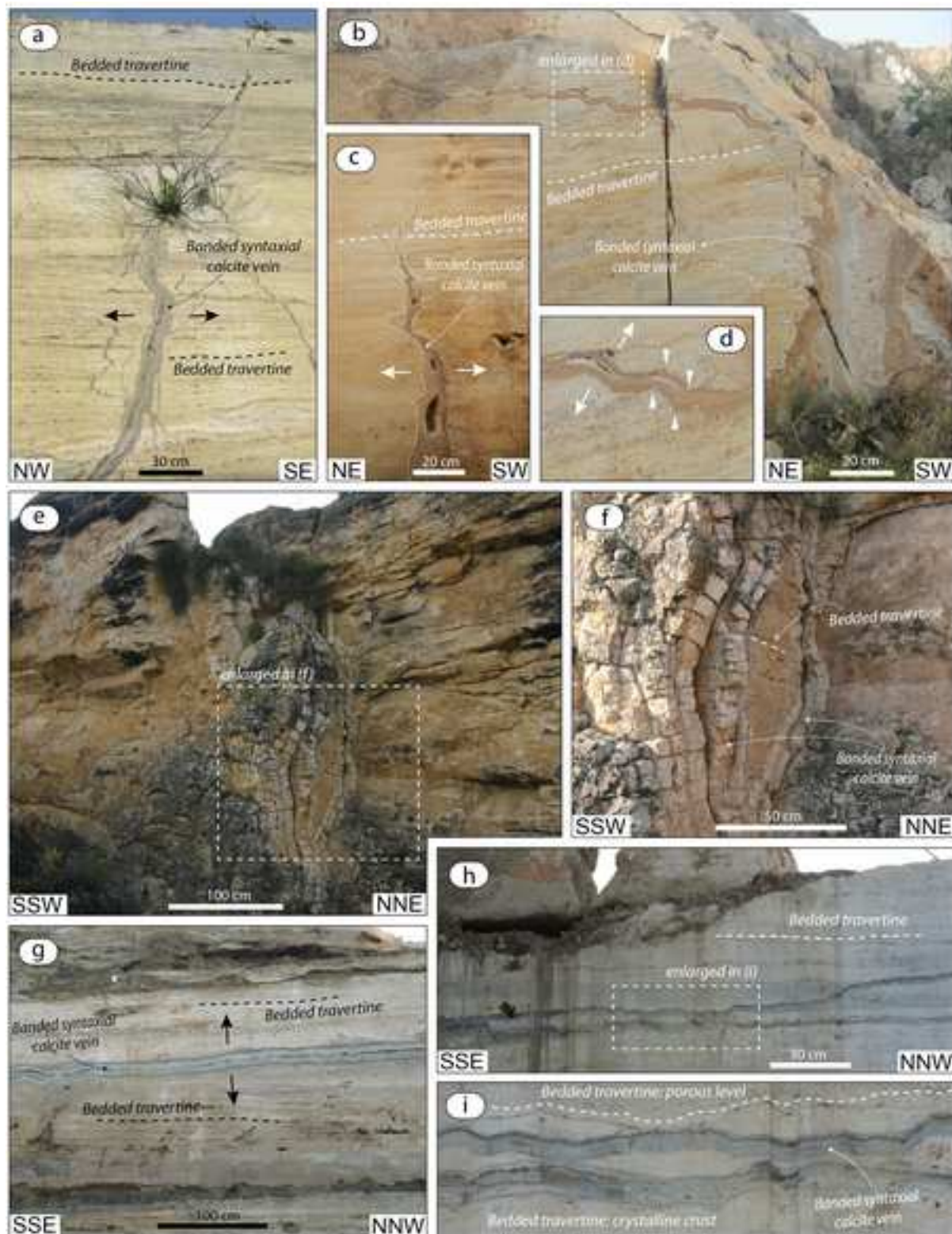


Fig. 3 - Examples of banded calcite veins filling cracks that cut across layers or follow bedding surfaces; a) banded calcite vein crossing late Pleistocene travertine layers at Bagno Vignoni (southern Tuscany, Italy); b) banded calcite veins system crossing a Pleistocene fissure ridge-type travertine deposit (Akköy fissure-ridge) in the Denizli Basin, southwestern Turkey; c) banded calcite vein filling a sub-vertical fracture in the wall of the Akköy fissure ridge (Denizli Basin, southwestern Turkey); d) detail of the inset indicated in (b); e) banded calcite veins system filling sub-vertical fractures crossing the middle Pleistocene fissure ridge-type travertine deposit (Çukurbağ fissure-ridge) in the Denizli Basin, southwestern Turkey; f) detail of the inset indicated in (e); g) sub-horizontal banded calcite vein filling a fracture sub-parallel to the bedding surfaces in the late Pleistocene-Holocene travertine deposits at Cava Campo Muri (Rapolano Terme, Italy); h) Sub-horizontal and low-angle banded calcite veins system filling a fracture that cut across layers or follow bedding surfaces in the Late-Pleistocene-Holocene travertine deposits at Cava Campo Muri (Rapolano Terme, Italy); i) detail of the inset indicated in (h).

Figure 4
[Click here to download high resolution image](#)

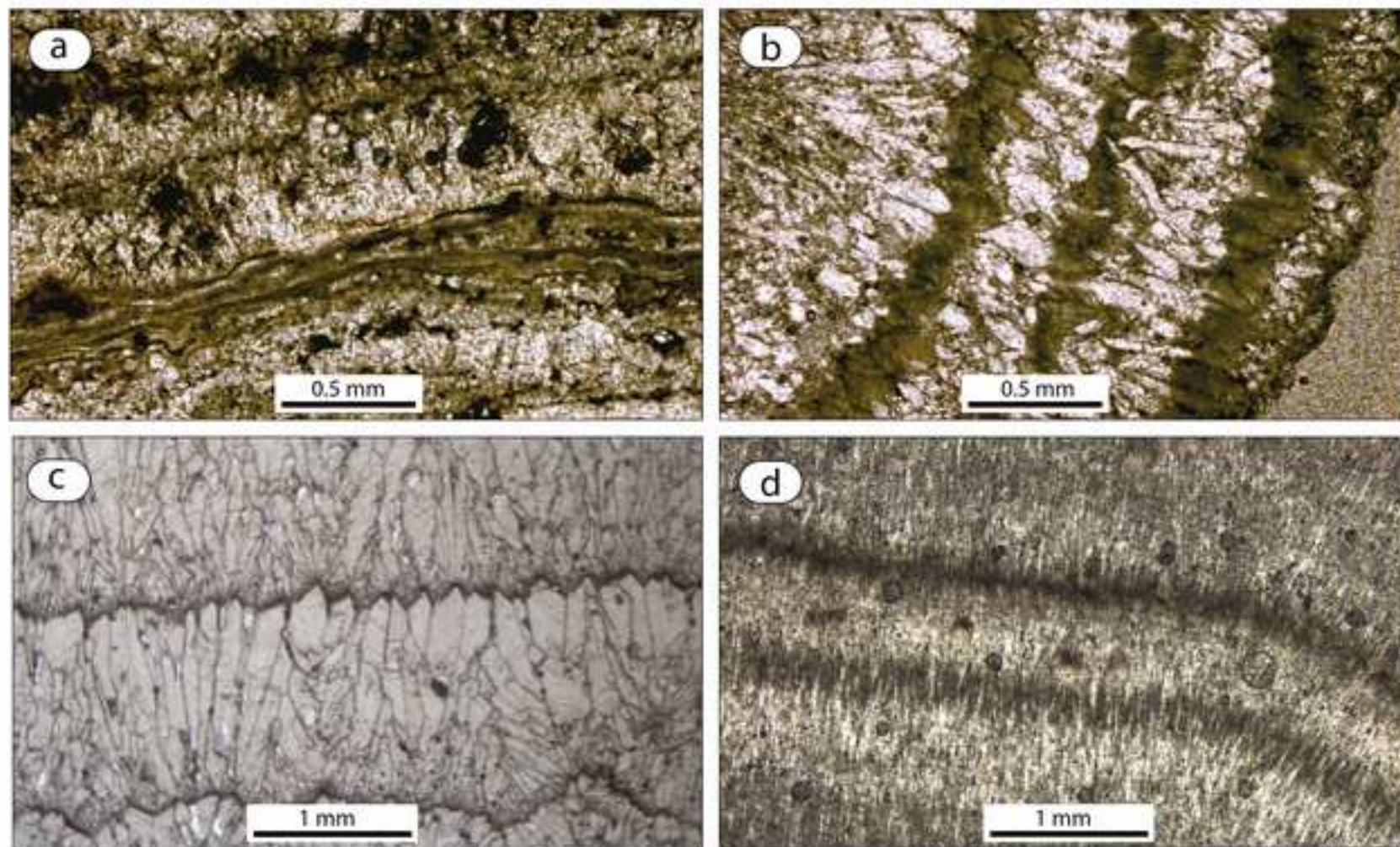


Fig. 4 - Photomicrographs of microfabrics of crystalline crusts and banded calcite veins filling fractures cutting across travertine beds. a-b) example of crystalline crust from Rapolano Terme (Italy); c-d) example of banded calcite vein from the Denizli Basin (Turkey). Please note the differences in fabric, dimension and crystal morphology. Many other examples of microfabrics are illustrated in numerous publications (Gandin and Capezzuoli, 2014; Della Porta, 2015; Croci et al., 2016; Della Porta et al., 2017 and references therein) to which the readers are addressed for more details.

Figure 5
[Click here to download high resolution image](#)

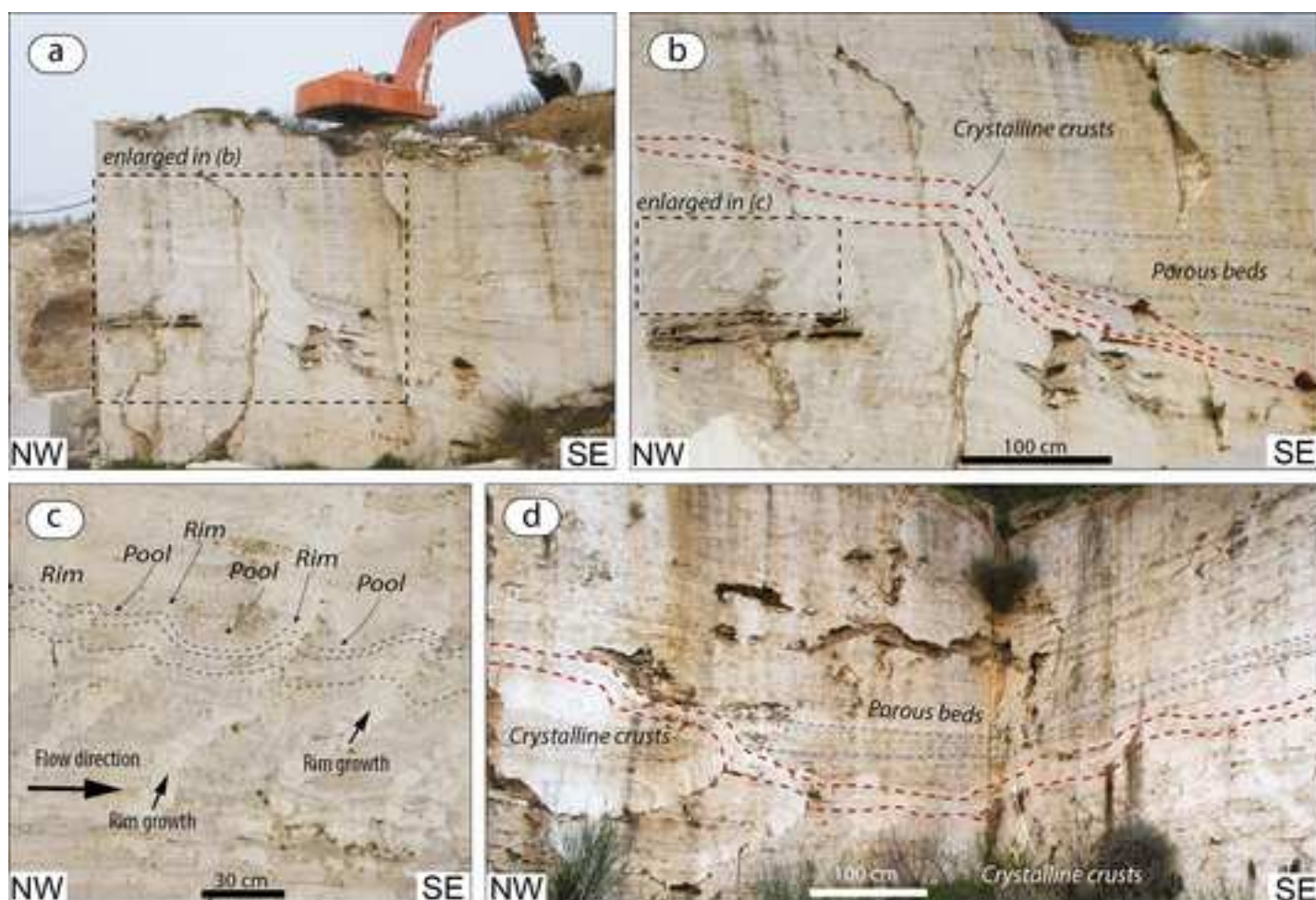


Fig. 5 - Photographs of saw-cut walls exposed in the Pianetti quarry near Saturnia (southern Tuscany, Italy), the same outcrops reported in Billi et al. 2017.
a-b) Slope deposit formed by crystalline crusts giving rise to terraces in a prograding pools system (the so-called “chimney-like veins” by Billi et al. 2017, enlarged in c) and the final slope accumulation. The slope deposit is unconformably overlain by subhorizontal porous strata formed by shrub facies (typical of subhorizontal pools) terminating in onlap against the slope depositional profile. c) Decimeter-scale pools and rims characterized by prograding and aggrading different fabric types. d) Cross-section of a progradational terraced slope with pools bordered by rounded rims prograding and aggrading. The terraced system is unconformably overlain by subhorizontal strata onlapping against the pool rims: this geometric configuration is a primary depositional feature and cannot be explained as a secondary features (i.e. the result of syn-diagenetic folds caused by laterally-confined volume expansion through hydrothermal incremental veining) as proposed by Billi et al. (2017) because the subhorizontal porous strata in onlap do not appear deformed by the alleged syn-diagenetic folding.

Figure 6
[Click here to download high resolution image](#)

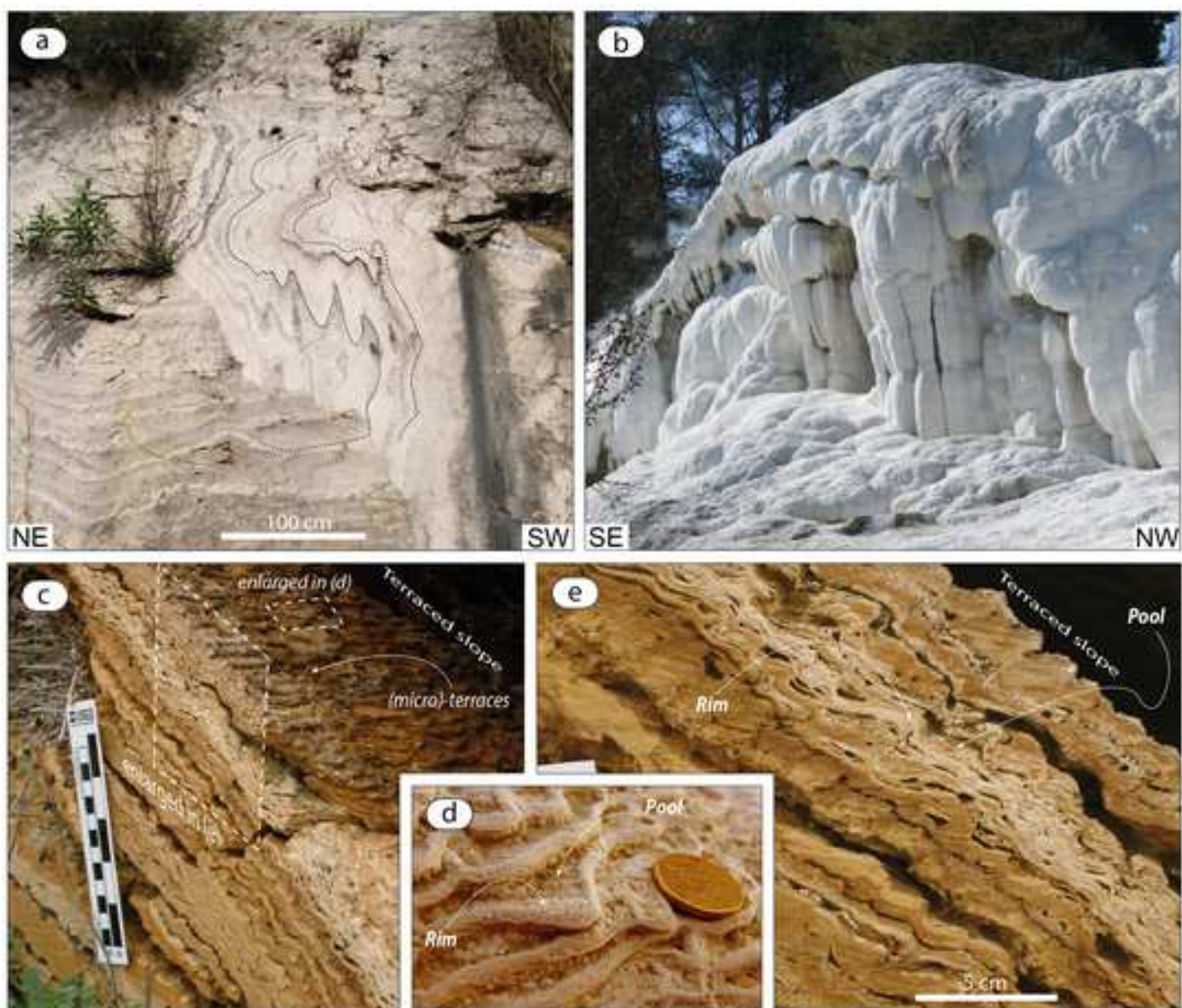


Fig. 6 – a) Irregular geometrical setting of travertine beds visible in saw-cut walls exposed in the Pianetti quarry near Saturnia (southern Tuscany, Italy), and interpreted by Billi et al. (2017) as the result of re-fold structures (cf their Fig. S10); b) Example of an active cascade travertine depositional system at Bagni San Filippo (southern Tuscany, Italy), where the sub-vertical slopes explain the geometrical setting of the travertine beds illustrated in (a) and interpreted by Billi et al. (2017) as secondary fold structures (i.e. refolded structures). c) Cross-section of a terraced slope; d) saw-tooth shape of travertine layers deriving from an orthogonal cross-section of the terraced slope: the saw-tooth shape is the result of the progradational growth of the microterraced slope.